IJE TRANSACTIONS C: Aspects Vol. 37 No. 09, (September 2024) 1812-1820

International Journal of Engineering

Journal Homepage: www.ije.ir

# Barrel-Spinning-Assisted Nickel Plating onto Copper in Sulphate Solution to Enhance Corrosion Resistance

F. B. Susetyo[a*], Y. A. Widiyanto[a], B. Soegijono[b], S. D. Yudanto[c], S. Ismarwanti[d], R. Kriswarini[d], C. Rosyidan[e]

[a] *Department of Mechanical Engineering, Universitas Negeri Jakarta, Jakarta, Indonesia*
[b] *PROUDTEK Lab, Department of Geoscience, Universitas Indonesia, Depok, Indonesia*
[c] *Research Center for Metallurgy, National Research and Innovation Agency, Serpong, Indonesia*
[d] *Research Center for Nuclear Material and Radioactive Waste Technology, National Research and Innovation Agency, Serpong, Indonesia*
[e] *Department of Petroleum Engineering, Universitas Trisakti, Jakarta, Indonesia*

*P A P E R I N F O*

*Paper history:*
Received 11 November 2023
Received in revised form 02 April 2024
Accepted 13 April 2024

*Keywords*:
*Film*
*Deposition Behavior*
*Physical Properties*
*Electrochemical Properties*

*A B S T R A C T*

Nickel (Ni) is an interesting candidate for corrosion protection of copper (Cu) due to its present passive area. Ni films with larger passive areas have better corrosion protection than those with smaller ones. In the present research, Ni films were produced over Cu. A barreling apparatus was employed to support the produced films in the sulphate solution. Various spinning speeds (0, 50, and 100 rpm) were used on the barrel while it was being processed. Several investigations were conducted, such as deposition rate, current efficiency, surface morphology, phase, film thickness, crystallographic orientation, and electrochemical properties. Increased spinning speed resulted in a decrease in the deposition rate, current efficiency, grain size, thickness, crystallite size, and exchange current density. Compared to a higher spinning speed, the decrease in spinning speed caused an increase in the oxygen content, surface roughness, and micro-strain. The higher speed of the barrel apparatus resulted in a lower corrosion rate Ni film of 0.147 mmpy. Moreover, the lower speed of the barrel apparatus resulted in a higher exchange current density Ni film of 0.997 A/cm².

***doi**: 10.5829/ije.2024.37.09c.11*

**NOMENCLATURE**

| | | | |
|---|---|---|---|
| $CV$ | Coefficient variant | $k$ | Crystallite-shape factor constant |
| $I_{corr}$ | Corrosion current density (A/cm$^2$) | $\lambda$ | Diffractometer radiation source (nm) |
| $K$ | Corrosion rate constant (3272 mmpy) | $D$ | Crystallite size (nm) |
| $EW$ | Equivalent weight (g) | $\varepsilon$ | Micro-strain value (%) |
| $\rho$ | Ni density (g/cm$^3$) | $\eta$ | Overpotential (V) |
| $A$ | Sample tested area (cm$^2$) | $a$ | Tafel intercept (V) |
| $\beta$ | Full width at half maximum (FWHM) value (°) | $b$ | Tafel slope (V/dec) |
| $\theta$ | Phase peak angle (°) | $J_0$ | Exchange current density (A/cm$^2$) |

## 1. INTRODUCTION

Nickel (Ni) and its alloy are significant materials for industrial applications, which include machine components. Moreover, Ni is an interesting candidate for corrosion protection of copper (Cu) due to its present passive area (1). The smaller passive areas of Ni films have less corrosion protection than the larger ones (2).

Several methods are conducted to fabricate Ni films, including electroplating, chemical vapor deposition (CVD), and physical vapor deposition (PVD) (3-5). Electroplating has a higher deposition rate than CVD and PVD (6). Moreover, electroplating is one of the lowest costs and eco-friendly to produce Ni films (7). There are two ways to hold a part during electroplating: rack and barrel (8). The choice is determined by the size of the

*Corresponding Author Email: fbudhi@unj.ac.id (F. B. Susetyo)

Please cite this article as: Susetyo FB, Widiyanto YA, Soegijono B, Yudanto SD, Ismarwanti S, Kriswarini R, Rosyidan C. Barrel-Spinning-Assisted Nickel Plating onto Copper in Sulphate Solution to Enhance Corrosion Resistance. International Journal of Engineering, Transactions C: Aspects. 2024;37(06):1812-20.

plated parts. Barreling plating is largely used in the industrial sector for small parts (9). The components are filled out into barrels, which spin in an electrolyte bath. More than 70 % of industrial plating facilities use the barrel technique to enable for full automation (10). Several advantages of the barrel are more solution transfer into a barrel, higher current density promoting a faster plating process, reduced electrolyte concentration, better plating for difficult alloy plating, and reduced drag-out (11).

Several scientific researches have found that current density, dosing electrolyte, and barrel rotation speed are several factors that influence the quality of film produced using plating. Sherwin et al. (12) investigated Ni plating using a Watts solution with varying current density, resulting in different surface morphologies and thicknesses. Leiden et al. (13) investigated how to control electrolyte dosing by using mathematical modeling and found that the approach was successful in validating the Zn-Ni barrel plating chain production process. Zhang (14) applied a modified Watt solution to deposit MCrAlX at a barrel speed of 7 rpm at 50 °C and a current density of 20 mA/cm$^2$. This resulted in the production of NiCrCoCrAlY, which has improved properties for cyclic oxidation and hot corrosion. Hong et al. (15) optimized barreling Ni-P plating by varying barreling speeds (1.5-4.5 rpm), resulting in different film properties.

Previous research has indicated that the presence of more salt in Ni baths makes waste treatment difficult (7). As a result, the current investigation employed a sulfate solution. Furthermore, three barrel speeds (0, 50, and 100 rpm) were utilized in this study. This research aims to investigate the properties of Ni films that were made using barreling plating. The investigation covered deposition rate, current efficiency, surface morphology, phase, film thickness, crystallographic orientation, and electrochemical properties.

## 2. EXPERIMENTAL METHODS

**2. 1. Material and Method** Electroplating of Ni on Cu substrates (1.5 × 1.5 cm) was conducted using a barreling apparatus in 0.5 M $NiSO_4$ solution (1500 ml). The electrolyte solution was prepared by mixing $NiSO_4$ with deionized water and stirring using a magnetic stirrer for around 30 minutes to achieve better homogeneity. Pure Cu and Ni were employed as the cathode and anode components, respectively. Prior to electrodeposition, the cathode was polished by abrasive paper and cleaned with acetone. Electrodeposition was performed using a DC power supply (MDB PS-305DM) with 25 mA of current for 2 h at 30 °C. The samples were plated at 0, 50, and 100 rpm of barreling rotating, namely NiB0, NiB50, and NiB100, respectively. The schematic apparatus for barreling plating is shown in Figure 1.

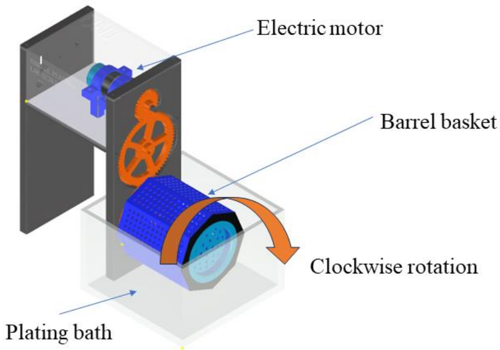


**Figure 1.** Ni barreling plating schematic apparatus

**2. 2. Characterization** The specimen was weighed prior to and after barreling plating. The mass increment was inserted into the previous research equation to calculate the deposition rate and current efficiency (1). Surface morphology, phase and film thickness were investigated using scanning electron microscope-energy dispersive spectroscopy (SEM-EDS) FEI Quanta 650. The investigation of surface roughness was carried out using MATLAB software and the captured SEM data was converted into grayscale (0 to 225) and histogram. Afterward, statistical analysis was employed to find the coefficient variant (CV) using the following equation (16).

$$CV\ (\%) = \frac{Standard\ deviation}{Average} \times 100 \quad (1)$$

PANalytical Xpert PRO was used for crystallographic orientation observations (Co K$\alpha$ = 1.79 Å, 40 kV, 15 mA) using step size 0.0217°. Using a Digi-Ivy DY 2311 in 3.5% NaCl solution at 30 °C (10 mV/s), electrochemical behavior, including open circuit potential (OCP), anodic polarization (AP), and cathodic polarization (CP), was investigated. Ni films as working electrode with 1 cm$^2$ tested surface area. Ag/AgCl and platinum are used as reference and counter electrodes. Corrosion rate (Cor. Rate) was calculated using the following equation (17).

$$Cor.rate\ (mmpy) = \frac{I_{corr} \times K \times EW}{\rho \times A} \quad (2)$$

## 3. RESULT AND DISCUSSIONS

**3. 1. Deposition Rate and Current Efficiency** The calculated deposition rate and current efficiency are shown in Figure 2. Since the barrel was not rotated, higher current efficiency reached around 94.95 %. It means that the combination between solution and current density is perfectly chosen. Ahmadzadeh et al. (18) reached 55% of electrodeposition efficiency when electrodeposited Ni at 24 °C using 30 mA/cm$^2$ of current density. Sherwin et al. (12) reach 100 % of current efficiency when Ni is electrodeposited using a Watts solution (30 °C). Ibrahim and Al Radadi (19) electrodeposed Ni using glycine as a complexing agent. Their results showed that increasing glycine concentration (from 0 to 125 g/l), pH (from 4 to 8), and $H_3BO_3$ (30 to 50 g/l) result in a decrease in current efficiency.

A higher deposition rate and current efficiency were observed in the NiB0 sample. They have a similar tendency; increasing the spinning speed decreases the values. The barrel rotation promoted stirring of the object and the plating solution (6). Therefore, the $Ni^{2+}$ ions species find it difficult to reach the surface of the cathode. Hence, the deposition rate and current efficiency decrease. Hili et al. (20) found that the current density influences the deposition rate; increasing the current density leads to an increase in deposition rate. Increased overpotential occurs when the current density is shifted to higher. $Ni^{2+}$ ions can break through an obstacle rapidly when current density accumulates to some extent. Therefore, the deposition rate is increased.

**3. 2. SEM-EDS and Film Thickness** The surface morphology investigation result is shown in Figure 3. Increasing speed of spinning facilitated the transition of pyramidal-like colonies to spherical colonies. A decrease in grain size was also caused by increasing the spinning speed. Compared to the deposition rate and current efficiency section, change to a spherical one and decrease the grain size due to the difficulty of $Ni^{2+}$ ion reaching the cathode's surface. Moreover, grain size is obviously related to the nucleation rate; a higher nucleation rate promotes the formation of smaller grain sizes (20).

The surface morphology investigation presents results that align with previous research (2). Sherwin et al. (12) found that increasing a current density increases current efficiency and promotes resulting wider grain size. Similar results were also found in Wasekar et al. (21) study. Wider grain sizes were formed due to decreased Ni cation concentrations at the electrolyte-cathode (21).

Figure 4 displays the results of the element investigation. The EDS measurement showed that the Ni film was perfectly added to the Cu substrate. Increasing the spinning speed promoted an increase in the oxygen content. As mentioned in previous research, many factors, such as sample transport, storage and electrolyte temperature, influenced the oxygen formation on the Ni surface (7). Therefore, further investigation is needed regarding the formation of oxygen in the present research.

The results of the film thickness investigation are shown in Figure 5. All films were deposited at similar times and in bath compositions. The thickness of the Ni

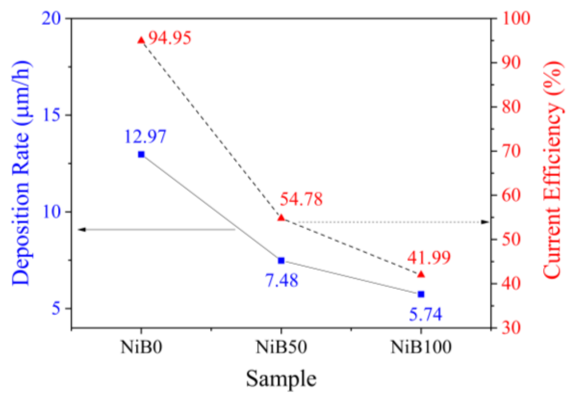


**Figure 2.** Deposition rate and current efficiency of Ni plating

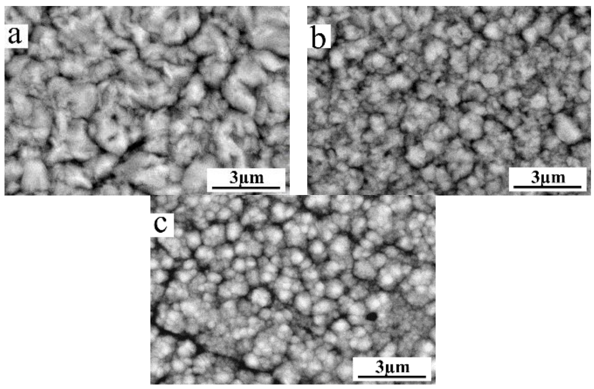


**Figure 3.** SEM capture of Ni films of a) NiB0, b) NiB50, and c) NiB100

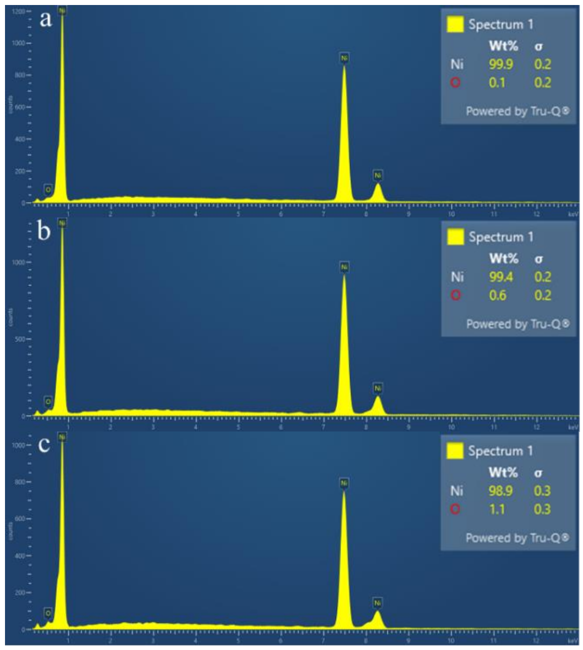


**Figure 4.** EDS result of Ni films of a) NiB0, b) NiB50, and c) NiB100

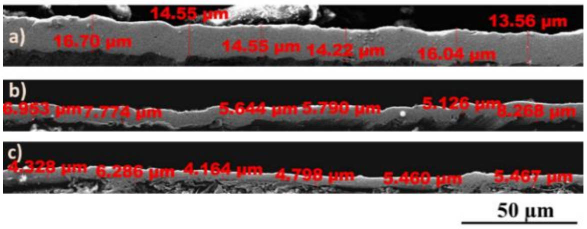


**Figure 5.** SEM cross-section of Ni films of a) NiB0, b) NiB50, and c) NiB100

film is reduced due to a decreased deposition rate. The average thickness of the film can be seen in Figure 6. The standard deviation of samples NiB0, NiB50 and NiB100 are 9.19, 7.18, and 4.93 µm, respectively. Hong et al. (15) conducted barreling electroless plating of Ni-P and found that plating thickness decreased with increasing barrel rotating speed (from 2.5 to 4.5 rpm) at 30 minutes of plating time.

**3. 3. Roughness Analysis** The surface roughness result is shown in Figure 7 and tabulated in Table 1. SEM micrograph is used to conduct roughness analysis using MATLAB. Increased spinning speed promoted an increase in roughness, confirmed by the CV value. The film surface becomes rougher as the CV value increases. This phenomenon is probably due to an increase nucleation rate, which increases roughness. Accelerated a nucleation rate promoted to increase grain growth (21). Another possibility is that the oxygen content of the Ni films is enhanced due to increasing the spinning speed, which promotes more surface roughness. Huntz et al. (22) study correlated oxidation and surface roughness dependent on time, resulting in more oxidation duration enhancing the surface roughness. Moreover, Bigos et al. (23) have found that side cathodic reactions of hydrogen influences decrease current efficiency and increase the roughness of the Ni film surface.

**3. 4. Crystallographic Orientation** XRD was used to investigate the formation of the Ni film on the Cu

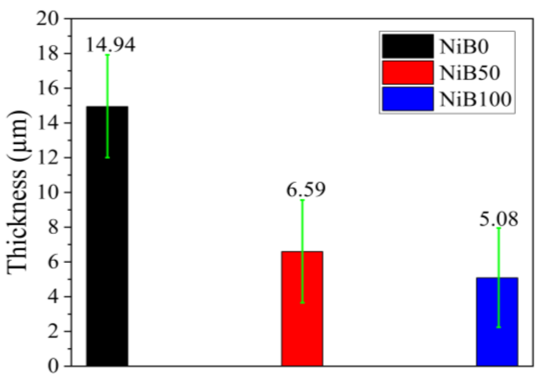


**Figure 6.** Average thickness of Ni films

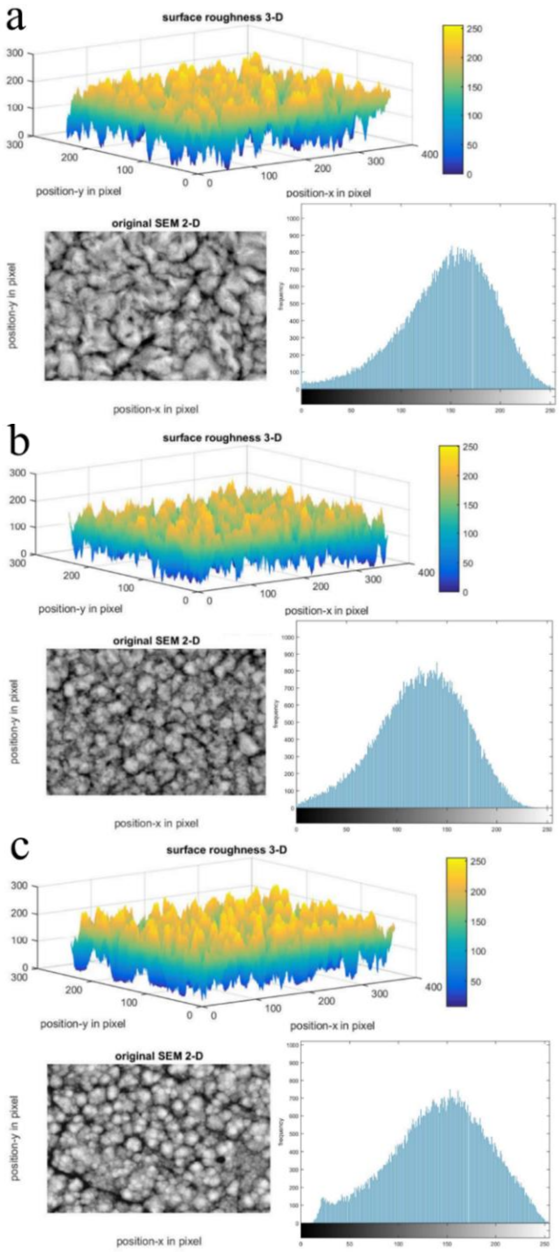


**Figure 7.** Surface roughness and histogram of Ni films of a) NiB0, b) NiB50, and c) NiB100

**TABLE 1.** Surface roughness analysis

| Sample | Average | Standard deviation | CV (%) |
|---|---|---|---|
| NiB0 | 146.37 | 45.93 | 31.38 |
| NiB50 | 124.77 | 42.76 | 34.27 |
| NiB100 | 141.64 | 49.41 | 34.89 |

substrate after the electrodeposition process. Figure 8 shows the Ni film diffractogram at 0, 50, and 100 rpm of the rotating barrel. The indexed plane peaks (111), (200), and (220) that represent the cubic Ni phase on a Cu substrate have been deposited. The Ni phase peaks correspond to several previous researches (7, 24). The diffraction pattern showed that the Cu substrate at the indexed plane peaks (111), (200), and (220) was also detected in the XRD test. The detector found the cubic Cu phase at angles of 50.79, 59.35, and 88.81° from a Co radiation source; these angles are similar to angles of 43.7, 50.7, and 74.3° from a Cu source (25).

The barreling rotating rate increases, resulting in a lower peak intensity of the Ni phase in (200) and (220) planes. Increasing barreling speed is inversely proportional to the peak intensity of the Ni phase, resulting in an increase in the peak of the Cu substrate phase. The SEM observation results (Figure 5) demonstrate that the thinner the Ni layer deposited, the higher the barrelling rate.

The Rietveld method was employed to calculate the lattice parameters of the Ni phase deposited on a Cu substrate using the diffraction pattern. The diffraction pattern of the calculation results compared to the observation results of the Ni films sample can be seen in Figure 9. The calculation data input utilizes cubic Ni and Cu phases with a space group of fm-3m. Using calculations, the a-lattice parameters of the Ni phase for samples NiB0, NiB50, and NiB100 were determined to be 0.3519, 0.3516, and 0.3518 nm, respectively. Table 2 shows the lattice parameters for all samples.

Using the Williamson-Hall plot method, the crystallite size estimate was calculated to determine how rotating barreling affects the crystallite size of Ni films. Williamson-Hall plot method with the following formula (7, 26).

$$\beta . \cos\theta = k\lambda D + 4\varepsilon \sin\theta \qquad (3)$$

Table 2 displays the β values of the Ni phase at the peaks of the (111), (200), and (220) planes. The plot of 4 sinθ vs. β cosθ of the Ni films is shown in Figure 10. This plot is used to generate straight line equations for each sample, as can be seen in the legend of Figure 10. The value of the straight-line equation is the microstrain value and the c value is the slope used to determine the crystal size. It can be seen from Table 2 that the higher the barreling rotating rate, the more crystal refinement occurs. SEM morphology observations in Figure 3 support this crystal refinement. The micro-strain of the Ni films sample increases when the barreling rotating rate is increased.

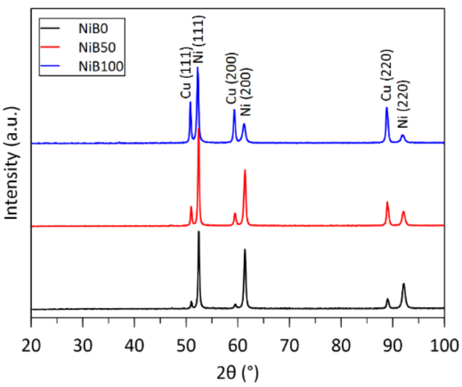

**Figure 8.** X-ray difractogram of the Ni films

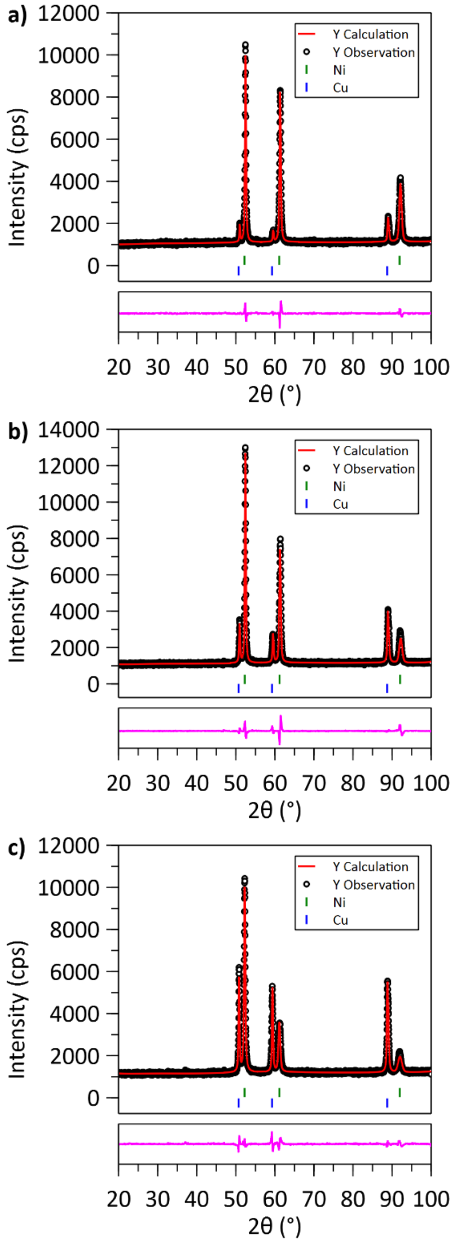

**Figure 9.** Plot of the observation pattern vs. calculation pattern of the Ni films a) NiB0, b) NiB50, and c) NiB100

**3. 5. Electrochemical Behavior** The OCP measurement in a 3.5% NaCl solution is shown in Figure 11. An increase in time measurement and $E_{OCP}$ has a positive effect on achieving a steady state in all samples. It can be assumed that oxide films form on the surface of

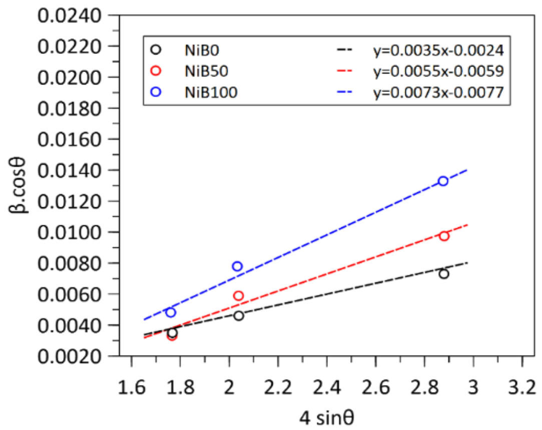


**Figure 10.** Plot of 4 sinθ vs. β cosθ of the Ni films

**TABLE 2.** Quantitatif analysis of Ni films

| Source | NiB0 | NiB50 | NiB100 |
|---|---|---|---|
| Lattice -a (nm) | 0.3519 | 0.3516 | 0.3518 |
| FWHM (111) (°) | 0.243 | 0.233 | 0.322 |
| FWHM (200) (°) | 0.321 | 0.404 | 0.527 |
| FWHM (220) (°) | 0.609 | 0.810 | 1.100 |
| D (nm) | 70.12 | 28.52 | 21.86 |
| ε (%) | 0.24 | 0.59 | 0.77 |

the Ni film and are promoted to form passive and protective films. On the contrary, it moves towards the negative direction, indicating the dissolution of the film (27). Generally, increasing the barreling spinning speed promoted a shift to the more positive OCP value at 300 s measurement. The NiB100 sample is nobler due to its more positive direction than others. The nobler sample has the advantage of more corrosion resistance due to less thermodynamic tendency to corrosion (28).

The AP measurement in 3.5 % NaCl is shown in Figure 12. Active, passive, and trans-passive regions are seen in various samples. Corrosion occurs in passive regions, oxide forming in passive regions such as NiO and starting of trans-passive regions indicating a value of the pitting potential ($E_{pit}$), which means aggressive species in 3.5 % NaCl penetrate the films (27). According to Khalid et al. (29) chloride ions could damage passive films.

By increasing the spinning speed, there was a shift towards a more positive pitting potential and a larger passive area. According to the EDS result, NiB100 has more oxygen, which is likely to result in a bigger passive region. A larger passive area is seen in the NiB100 sample, promoting better surface protection. More negative $E_{pit}$ is shown in the NiB0 sample promoted to easier form pitting in the Ni surface.

The AP result is shown in Table 3. Tafel extrapolation methods found corrosion potential ($E_{corr}$) and corrosion current density ($I_{corr}$), and then the corrosion rate was found using expression (2). Increasing the spinning speed promoted a shift to more positive corrosion potential values. Moreover, an increase in a corrosion current density increases the corrosion rate. The lower corrosion rate is seen in the sample NiB100, probably due to a larger passive area and nobler. Raghupathy et al. (30) found that the nobler sample tends to lower the corrosion rate. Moreover, Basori et al. (27) found that a larger passive area promoted more protection for the test specimen and led to a lower corrosion rate.

Wider grain size also contributes to the corrosion rate. Mahmood et al. (31) have found film with smaller grain size is lower porosity promoted to decreasing the corrosion rate. Compared to the SEM result, it can be seen that a small grain size is found in the NiB100; therefore, it has a lower corrosion rate.

Figure 13 shows the CP curve of samples in 3.5 % NaCl at 30 °C (sweep potential range from 0 to -1.3 V vs Ag/AgCl). The NiB0 and NiB50 showed a small onset

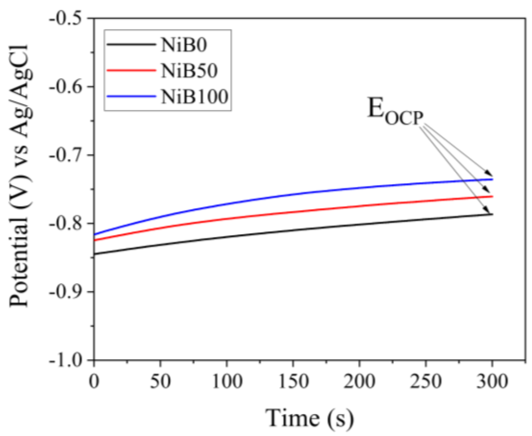


**Figure 11.** OCP measurement result of NiB0, NiB50, and NiB100

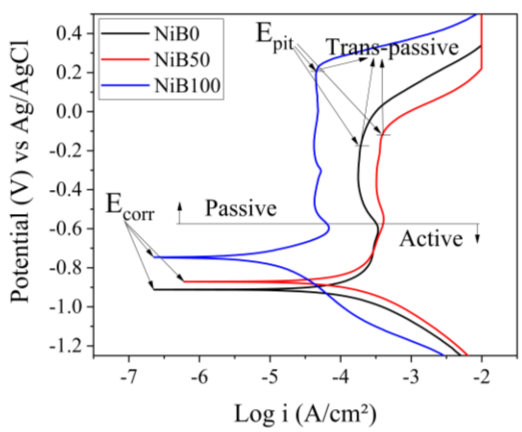


**Figure 12.** AP curve of NiB0, NiB50 and NiB100

**TABLE 3.** AP measurement result

| Sample | $E_{corr}$ (V) vs Ag/AgCl | $I_{corr}$ (A/cm$^2$) | Cor. rate (mmpy) |
|---|---|---|---|
| NiB0 | -0.912 | $1.45\times10^{-4}$ | 1.56 |
| NiB50 | -0.870 | $1.69\times10^{-4}$ | 1.82 |
| NiB100 | -0.745 | $1.36\times10^{-5}$ | 0.147 |

**TABLE 4.** Kinetic parameters of the HER on NiB0, NiB50 and NiB100

| Sample | a (V) | b (V/dec) | η (V) | $J_0$ (A/cm²) |
|---|---|---|---|---|
| NiB0 | 0.040 | 26.79 | -0.940 | 0.997 |
| NiB50 | 0.050 | 22.71 | -1.007 | 0.995 |
| NiB100 | 0.052 | 21.78 | -1.024 | 0.994 |

overpotential of -0.940 and -1.007 V, which was shifted to more positive than the NiB100 sample (-1.024 V) for the hydrogen evolution reaction (HER). Small onset potential indicates higher HER activation energy (32). Ng et al. (32) stated the onset potential was defined as a point where the corrected reduction current deviated from the baseline with more than 1 mA/cm$^2$.

Tafel plots of various samples were recorded with the linear regions fitted into the following Tafel equation (33), shown in Figure 14.

$$\eta = a + b \log J_0 \qquad (4)$$

The Tafel intercept and Tafel slope of HER for all samples can be seen in Table 4. Shifting to a higher

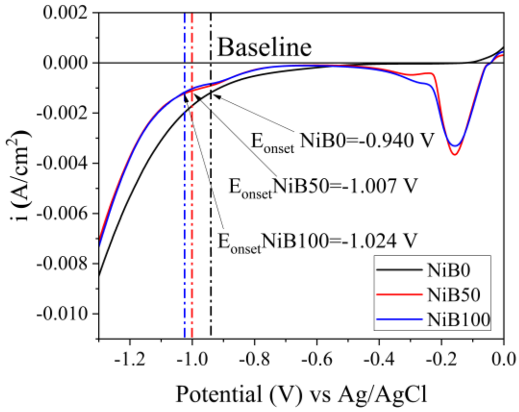


**Figure 13.** CP curve of NiB0, NiB50 and NiB100

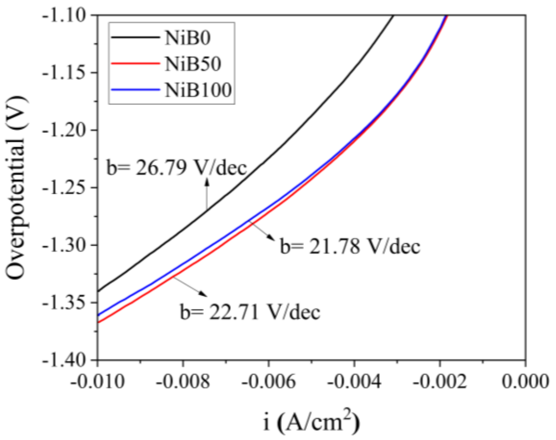


**Figure 14.** Tafel plots of NiB0, NiB50, and NiB100

spinning magnet increases the intercept and decreases the Tafel slope. Protsenko et al. (33) stated Tafel intercept is dependent to the exchange current density. Moreover, the following equation could calculate the exchange current density (33).

$$\log(J_0) = -\frac{a}{b} \qquad (5)$$

The exchange current density values for NiB0, NiB50, and NiB100 with a deposition time of 2 hours are presented in Table 4. The exchange current density values were 0.997, 0.995, and 0.994 A/cm² for NiB0, NiB50, and NiB100, respectively. With the increased spinning speed, the promoting exchange current density decreased, affecting hydrogen production less efficiently on film surfaces. The higher exchange current density indicates the best hydrogen production (34).

Xie et al. (35) found porous Ni has less charge transfer resistance and the highest exchange current density. Lowest charge transfer resistance, indicating films more easily corroded (27). It seems that corrosion resistance correlates with exchange current density. When corrosion resistance is lower, the exchange current density is higher. Nikolic et al. (36) found that shifting to a lower charge transfer resistance promoted a higher exchange current density. Compared to the AP and CP results, a higher corrosion rate and exchange current density are seen in the NiB0 sample, which perfectly agrees with the Nikolic et al. (36) report, which means the NiB0 sample is easy to corrode but has higher hydrogen production.

## 4. CONCLUSSIONS

Ni films made of barreling plating techniques were successfully made. Increasing spinning speed decreases deposition rate, current efficiency, grain size and film thickness due to $Ni^{2+}$ ions species' difficulty reaching the cathode's surface. In contrast, decreasing spinning speed increases oxygen content, surface roughness, and micro-strain. The accelerated nucleation rate promoted increasing the roughness of the film. Moreover, increased oxygen content resulted in a larger passive area and nobler film. A larger passive area, more noble, and less grain size are seen in the NiB100 sample, promoting better surface protection and less corrosion rate. When corrosion resistance is lower, the exchange current density is higher. The higher exchange current density indicates the best hydrogen production.

## 5. ACKNOWLEDGEMENT

The authors gratefully thank the BLU POK Engineering Faculty, Universitas Negeri Jakarta, for a research grant with contract number (866/UN39/HK.02/2023-Rector) and (T/027/5.FT/Kontrak-Penelitian/PT.01.03/III/2023-Dean).

## 6. REFERENCES

1. Soegijono B, Susetyo F, editors. Magnetic field exposure on electroplating process of ferromagnetic nickel ion on copper substrate. Journal of Physics: Conference Series; 2022: IOP Publishing.
2. Susetyo FB, Faridh A, Soegijono B, editors. Stirring Effect on Surface Morphology, Structure, and Electrochemical Behavior of Electrodeposited Nickel Film on Copper Substrates. IOP Conference Series: Materials Science and Engineering; 2019: IOP Publishing.
3. Ghorbani H, Poladi A. Md-simulation of duty cycle and tan interlayer effects on the surface properties of ta coatings deposited by pulsed-dc plasma assisted chemical vapor deposition. International Journal of Engineering, Transactions B: Applications,. 2020;33(5):861-9. https://doi.org/10.5829/IJE.2020.33.05B.18
4. Poursaeidi E, Salarvand A. Comparison of properties of ti/tin/ticn/tialn film deposited by cathodic arc physical vapor and plasma-assisted chemical vapor deposition on custom 450 steel substrates. International Journal of Engineering, Transactions A: Basics. 2016;29(10):1459-68. https://doi.org/10.5829/idosi.ije.2016.29.10a.17
5. Toghraei M, Siadati H. Electrodeposited co-pi catalyst on α-Fe2O3 photoanode for water-splitting applications. International Journal of Engineering, Transactions C: Aspects. 2018;31(12):2085-91. 10.5829/ije.2018.31.12c.13
6. Miyake M, Kita T, Ikenoue T, Hirato T. Aluminum Barrel Plating on Steel Bolts Using Chloroaluminate Ionic Liquids. Journal of The Electrochemical Society. 2022;169(7):072509. https://doi.org/10.1149/1945-7111/ac82ca
7. Syamsuir S, Soegijono B, Yudanto SD, Basori B, Ajiriyanto MK, Nanto D, et al. Electrolyte temperature dependency of electrodeposited nickel in sulfate solution on the hardness and corrosion behaviors. International Journal of Engineering, Transactions C: Aspects,. 2023;36(6):1193-200. https://doi.org/10.5829/IJE.2023.36.06C.18
8. Fayomi O, Akanade I, Sode A, editors. A Review on the Efficacy of Electroplating in Deteriorating Environments. Journal of Physics: Conference Series; 2019: IOP Publishing.
9. Böttcher R, Valitova A, Ispas A, Bund A. Electrodeposition of aluminium from ionic liquids on high strength steel. Transactions of the IMF. 2019;97(2):82-8. https://doi.org/10.1080/00202967.2019.1573941
10. Leiden A, Herrmann C, Thiede S. Cyber-physical production system approach for energy and resource efficient planning and operation of plating process chains. Journal of cleaner production. 2021;280:125160. https://doi.org/10.1016/j.jclepro.2020.125160
11. Sullivan GP, Hyner R, Masella P. The NICE3-Whyco technologies partnership: saving energy, dollars, and the environment in the metal plating industry. Resources, conservation and recycling. 2000;28(3-4):199-205. https://doi.org/10.1016/S0921-3449(99)00044-0
12. Sherwin C. Effects of Current Density on Surface Morphology and Coating Thickness of Nickel Plating on Copper Surface. Turkish Journal of Computer and Mathematics Education (TURCOMAT). 2021;12(10):79-83.
13. Leiden A, Kölle S, Thiede S, Schmid K, Metzner M, Herrmann C. Model-based analysis, control and dosing of electroplating electrolytes. The International Journal of Advanced Manufacturing Technology. 2020;111(5):1751-66. https://doi.org/10.1007/s00170-020-06190-0
14. Zhang Y. Development of Marinized Pt-Modified MCrAlX Coatings with Improved Hot Corrosion and Oxidation Resistance Synthesized via a Low-Cost Electrodeposition Process. 2019.
15. Hong IK, Kim H, Lee SB. Optimization of barrel plating process for electroless Ni–P plating. Journal of Industrial and Engineering Chemistry. 2014;20(5):3767-74. https://doi.org/10.1016/j.jiec.2013.12.077
16. Rwawiire S, Kasedde A, Nibikora I, Wandera G. Prediction of polyester/cotton ring spun yarn unevenness using adaptive neuro Fuzzy inference system. Journal of Textile and Apparel, Technology and Management. 2014;8(4).
17. Prasai D, Tuberquia JC, Harl RR, Jennings GK, Bolotin KI. Graphene: corrosion-inhibiting coating. ACS nano. 2012;6(2):1102-8. https://doi.org/10.1021/nn203507y
18. Ahmadzadeh M, Almasi-Kashi M, Ramazani A, Montazer A. Electrodeposition efficiency of Ni in the fabrication of highly ordered nanowire arrays: The roles of Cu pre-plating and barrier layer temperature. Applied Surface Science. 2015;356:687-94. https://doi.org/10.1016/j.apsusc.2015.08.104
19. Ibrahim MA, Al Radadi RM. Role of glycine as a complexing agent in nickel electrodeposition from acidic sulphate bath. International Journal of Electrochemical Science. 2015;10(6):4946-71. https://doi.org/10.1016/s1452-3981(23)06678-6
20. Hili K, Fan D, Guzenko VA, Ekinci Y. Nickel electroplating for high-resolution nanostructures. Microelectronic Engineering. 2015;141:122-8. https://doi.org/10.1016/j.mee.2015.02.031
21. Wasekar NP, Haridoss P, Seshadri S, Sundararajan G. Influence of mode of electrodeposition, current density and saccharin on the microstructure and hardness of electrodeposited nanocrystalline nickel coatings. Surface and Coatings Technology. 2016;291:130-40. https://doi.org/10.1016/j.surfcoat.2016.02.024
22. Huntz AM, Lefevre B, Cassino F. Roughness and oxidation: application to NiO growth on Ni at 800 C. Materials Science and Engineering: A. 2000;290(1-2):190-7. https://doi.org/10.1016/S0921-5093(00)00944-8
23. Bigos A, Wolowicz M, Janusz-Skuza M, Starowicz Z, Szczerba MJ, Bogucki R, et al. Citrate-based baths for electrodeposition of nanocrystalline nickel coatings with enhanced hardness. Journal of Alloys and Compounds. 2021;850:156857. https://doi.org/10.1016/j.jallcom.2020.156857
24. Zhang C, Liu H, Ju P, Zhu L, Li W. Effects of pH on the Nickel coating microstructure and internal stress from an additive-free watts-type bath with phytic acid. Journal of The Electrochemical Society. 2018;165(11):D518. https://doi.org/10.1149/2.0451811jes
25. Betancourt-Galindo R, Reyes-Rodriguez P, Puente-Urbina B, Avila-Orta C, Rodríguez-Fernández O, Cadenas-Pliego G, et al. Synthesis of copper nanoparticles by thermal decomposition and their antimicrobial properties. Journal of Nanomaterials. 2014;2014:10-. https://doi.org/10.1155/2014/980545
26. Yudanto SD, Dewi YP, Sebayang P, Chandra SA, Imaduddin A, Kurniawan B, et al. Influence of CNTs addition on structural and

superconducting properties of mechanically alloyed MgB 2. Journal of Metals, Materials and Minerals. 2020;30(3). https://doi.org/10.14456/jmmm.2020.32

27. Basori B, Mohamad WM, Mansor MR, Tamaldin N, Iswandi A, Ajiriyanto MK, et al. Effect of KOH concentration on corrosion behavior and surface morphology of stainless steel 316L for HHO generator application. Journal of Electrochemical Science and Engineering. 2023;13(3):451-67. http://dx.doi.org/10.5599/jese.1615

28. Song D, Li C, Liang N, Yang F, Jiang J, Sun J, et al. Simultaneously improving corrosion resistance and mechanical properties of a magnesium alloy via equal-channel angular pressing and post water annealing. Materials & Design. 2019;166:107621. https://doi.org/10.1016/j.matdes.2019.107621

29. Khalid MA, Miyazato S, Minato T, Mizuguchi H. Effect of Silane and Silicate based Penetrants against Corrosion of Steel with Partial Cover Thickness. Civil Engineering Journal. 2023;9(12):2970-88. https://doi.org/10.28991/CEJ-2023-09-12-02

30. Raghupathy Y, Natarajan K, Srivastava C. Microstructure, electrochemical behaviour and bio-fouling of electrodeposited nickel matrix-silver nanoparticles composite coatings on copper. Surface and Coatings Technology. 2017;328:266-75. https://doi.org/10.1016/j.surfcoat.2017.08.068

31. Mahmood M, Suryanto S, Al Hazza M, Haidera F. Developing of corrosion resistance nano copper oxide coating on copper using anodization in oxalate solution. International Journal of Engineering, Transactions B: Applications,. 2018;31(3):450-5. https://doi.org/10.5829/ije.2018.31.03c.07

32. Ng CH, Winther-Jensen O, Ohlin CA, Winther-Jensen B. Exploration and optimisation of poly (2, 2′-bithiophene) as a stable photo-electrocatalyst for hydrogen production. Journal of Materials Chemistry A. 2015;3(21):11358-66. https://doi.org/10.1039/c5ta00291e

33. Protsenko V, Bobrova L, Butyrina T, Danilov F. Hydrogen evolution reaction on Cr–C electrocatalysts electrodeposited from a choline chloride based trivalent chromium plating bath. Вопросы химии и химической технологии. 2019(1):61-6. https://doi.org/10.32434/0321-4095-2019-122-1-61-66

34. Huang Y-g, Fan H-l, Chen Z-k, Gu C-b, Sun M-x, Wang H-q, et al. The effect of graphene for the hydrogen evolution reaction in alkaline medium. International Journal of hydrogen energy. 2016;41(6):3786-93. https://doi.org/10.1016/j.ijhydene.2015.12.113

35. Xie Z, He P, Du L, Dong F, Dai K, Zhang T. Comparison of four nickel-based electrodes for hydrogen evolution reaction. Electrochimica acta. 2013;88:390-4. https://doi.org/10.1016/j.electacta.2012.10.057

36. Nikolic VM, Maslovara SL, Tasic GS, Brdaric TP, Lausevic PZ, Radak BB, et al. Kinetics of hydrogen evolution reaction in alkaline electrolysis on a Ni cathode in the presence of Ni–Co–Mo based ionic activators. Applied Catalysis B: Environmental. 2015;179:88-94. https://doi.org/10.1016/j.apcatb.2015.05.012



## Persian Abstract

**چکیده**

نیکل (Ni)یک کاندید جالب برای محافظت در برابر خوردگی مس (Cu)به دلیل منطقه غیرفعال فعلی آن است. فیلم‌های نیکل با مناطق غیرفعال بزرگ‌تر، در برابر خوردگی بهتری نسبت به فیلم‌های کوچک‌تر دارند. در تحقیق حاضر فیلم‌های Ni بر روی مس تولید شدند. یک دستگاه بشکه برای حمایت از فیلم های تولید شده در محلول سولفات استفاده شد. سرعت چرخش مختلف (۰، ۵۰ و ۱۰۰ دور در دقیقه) روی بشکه در حین پردازش استفاده شد. تحقیقات متعددی مانند نرخ رسوب، بازده جریان، مورفولوژی سطح، فاز، ضخامت فیلم، جهت کریستالوگرافی و خواص الکتروشیمیایی انجام شد. افزایش سرعت چرخش منجر به کاهش نرخ رسوب، راندمان جریان، اندازه دانه، ضخامت، اندازه کریستالیت و چگالی جریان مبادله شد. در مقایسه با سرعت چرخش بالاتر، کاهش سرعت چرخش باعث افزایش محتوای اکسیژن، زبری سطح و ریز کرنش شد. سرعت بالاتر دستگاه بشکه منجر به کاهش خوردگی فیلم نیکل به میزان ۰.۱۴۷ میلی‌متر بر اینچ شد. علاوه بر این، سرعت پایین دستگاه بشکه منجر به یک فیلم نیکل با چگالی جریان تبادلی بالاتر ۰.۹۹۷ $A/cm^2$ شد.